AIAA JOURNAL
Vol. 35, No. 6, June 1997

Detailed Investigation of the Three-Dimensional Separation About a 6:1 Prolate Spheroid

Christopher J. Chesnakas*
David Taylor Model Basin, U.S. Naval Surface Warfare Center, West Bethesda, Maryland 20817-5700
and
Roger L. Simpson†
Virginia Polytechnic Institute and State University, Blacksburg, Virginia 24061-0203

The flow in the crossflow separation region of a 6:1 prolate spheroid at 10- and 20-deg angle of attack, $Re_L = 4.20 \times 10^6$, was investigated using a novel, miniature, three-dimensional, fiber-optic laser Doppler velocimeter (LDV). The probe was used to measure three simultaneous, orthogonal velocity components from within the model, and these measurements were simultaneous with wall-pressure measurements made just below the LDV probe volume. The LDV measurements extend from approximately $y^+ = 7$ out to beyond the boundary-layer edge. The design and operation of this LDV probe is summarized. Plots of velocity, skin friction, wall-flow angle, mean and fluctuating pressures, turbulent kinetic energy, helicity density, and secondary streamlines are used to show the location of separation and reattachment lines. These measurements are also used to show that a trough of fluid, which is quite distinct from the rest of the flow, exists just downstream of the separation sheet. This trough has fluid of very low mean and turbulent kinetic energy. Plots of the turbulence anisotropy show there to be little correlation between the flow-gradient and the turbulent-shear-stress angles over large regions of the flow. This implies that turbulence models employing the eddy viscosity concept cannot be adapted to three-dimensional separated flows such as this.

Nomenclature

C_f = skin-friction coefficient, $\tau_w / (\rho U^2/2)$
C_p = pressure coefficient, $(P - P_s)/(P_t - P_s)$
h = helicity density, $\omega \cdot U$
L = length of model, 1.37 m
P = mean pressure
P_s = tunnel static pressure
P_t = tunnel total pressure
p = fluctuating component of pressure
Q = tunnel head
q^2 = fluctuating component of the velocity, $\overline{u^2} + \overline{v^2} + \overline{w^2}$
Re = Reynolds number
U = velocity component in a plane parallel to the wall, in the axial direction
U_{wc} = velocity component in a plane parallel to the wall, in the direction of the flow at the wall
U_∞ = wind-tunnel freestream velocity
V = velocity component normal to the wall
W = velocity component in a plane parallel to the wall, perpendicular to the axial direction (positive in the direction of increasing ϕ)
x = axial distance from the nose of model
y = perpendicular distance from the model surface
α = model angle of attack to incoming flow
β = flow angle, in plane perpendicular to y, from the axial direction (positive in the windward direction)
γ_g = flow gradient angle
γ_τ = turbulent-shear-stress angle
ϕ = circumferential coordinate, from windward side
ω = vorticity

Introduction

THE phenomenon of three-dimensional separation of the turbulent flow about a body, though quite common, is both difficult to model and poorly understood. Indeed, since—unlike in two-dimensional flow separation—three-dimensional flow separation is rarely associated with the vanishing of the wall shear stress, it can often be difficult to even identify the presence or precise location of three-dimensional flow separation.

To better understand three-dimensional flow separation, several groups have studied the flow about a 6:1 prolate spheroid at angle of attack. This flow is a well-defined, relatively simple three-dimensional flow, which exhibits all of the fundamental phenomena of three-dimensional flow, and is shown schematically in Fig. 1. The flow around the prolate spheroid separates on the lee side of the body and forms a surface that rolls up into the primary vortex. At a point aft of the primary separation, a secondary separation occurs, which rolls up into the secondary vortex located underneath the primary vortex. The actual existence of the secondary separation, or possibly even a tertiary separation, depends on flow conditions. These separations result in a highly skewed and, thus, three-dimensional boundary layer.

Previous works by Meier et al.,[1,2] Kreplin et al.[3] and Vollmers et al.[4] at the DFVLR (now the DLR, German Aerospace Research Establishment) have documented the surface flow, surface pressure, skin friction, and mean velocity around the prolate spheroid. Previous work at Virginia Polytechnic Institute (VPI) by Ahn[5] has documented the Reynolds number and angle-of-attack effects on the boundary layer transition and separation phenomena for this flow. Barber and Simpson[6] thoroughly documented the mean and turbulent velocities in the crossflow separation region, but due to the limitations of their instrumentation (five-hole pressure probes and crossed hot wires) they obtained no data within the inner boundary layer.

Because of the simple geometry and the extent of the experimental data, this flowfield has made an excellent test case for three-dimensional computational models. A recent study by AGARD[7] used the DFVLR data for comparison to three-dimensional computations utilizing integral boundary-layer, algebraic mixing-length, and eddy-viscosity turbulence models. The AGARD study found that all of the computational models experienced difficulties in calculating the flowfield in the crossflow separation region. Gee et al.[8] were able to get somewhat better results calculating the flow about the 6:1 prolate spheroid using versions of the Baldwin–Lomax and Johnson–King turbulence models modified for three dimensions, but stated that "more experimental data may be required before a

Received Aug. 8, 1996; revision received Feb. 26, 1997; accepted for publication March 3, 1997.

*Mechanical Engineer, Carderock Division, Code 5400, 9500 MacArthur Boulevard. Member AIAA.
†Jack E. Cowling Professor, Department of Aerospace and Ocean Engineering, 215 Randolph Hall. Fellow AIAA.

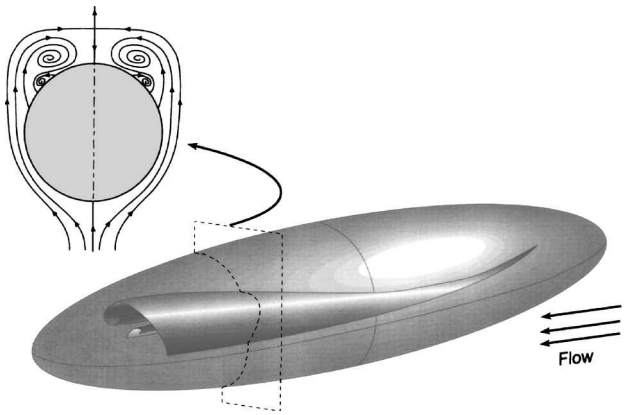

Fig. 1 Crossflow separation on the prolate spheroid.

better understanding of the effects of turbulence models on flow parameters can be gained."

The effects of the three dimensionality on the turbulence in the boundary layer of the 6:1 prolate spheroid were investigated in detail in Ref. 9. In that paper, all three velocity components, Reynolds stresses, and velocity triple products were measured from the viscous sublayer to beyond the boundary-layer edge near the separation line on the prolate spheroid. These measurements were used to calculate all important terms in the turbulent kinetic energy (TKE) equation and to show how the balance of turbulent convection, diffusion, production, dissipation, and viscous diffusion varied throughout the three-dimensional boundary layer. The paper also showed how the assumptions of various turbulence models were not supported by the measured flow conditions about the prolate spheroid. That study, however, focused on only one location ($x/L = 0.762$, $\phi = 123$ deg) at one angle of attack (10 deg).

The present work builds on the earlier works of Chesnakas and Simpson[9,10] and Chesnakas et al.[11] and extends the knowledge of this three-dimensional separated flow by presenting a fuller set of the data obtained about the prolate spheroid, data at several axial locations and at two angles of attack, and by explaining how the separation develops. The aim of this paper, then, is to put the earlier detailed investigation of the turbulence structure about the prolate spheroid in perspective by showing how the vortices associated with three-dimensional separation develop on the prolate spheroid and how the separations and reattachments associated with these vortices effect the boundary layer. This will also lay the groundwork for future interrogations of this data set concerning the modeling of the Reynolds stress transport equations and the modeling of velocity triple products.

The present measurements were accomplished using a miniature, three-dimensional, fiber-optic laser Doppler velocimeter (LDV) designed specifically for this application. The probe was placed within the model, and all beams passed through a plastic window molded to the shape of the model so that the flow was virtually undisturbed by the instrumentation. The probe was configured to measure three simultaneous, orthogonal velocity components. In this way, the total velocity vector and Reynolds stress tensor were obtained with maximum accuracy. A pressure tap was placed in the window almost directly below the measurement volume so that pressure measurements could be made simultaneously with the velocity measurements. The full set of velocity measurements about the prolate spheroid is too voluminous to report here but can be found in Ref. 11 and in the data bank contribution of Chesnakas and Simpson.[9]

Experimental Facility

Tests were performed in the VPI and State University stability wind tunnel. This tunnel is a continuous, closed-test-section, single-return, subsonic wind tunnel with a 7-m-long, 1.8-m square test section. The 9:1 contraction ratio and seven antiturbulence screens provide for very low-turbulence levels, on the order of 0.03% or less. Temperature stabilization is provided by an air exchange tower.

The 6:1 prolate spheroid model used in this experiment is 1.37 m (54 in.) in length and 0.229 m (9 in.) in diameter. The model has a fiberglass skin bonded to an aluminum frame. Windows 30 × 150 × 0.75 mm thick were placed in the skin for optical access to the flow. The windows were molded to the curvature of the model to minimize flow disturbances and were mounted flush with the model surface within 0.1 mm. Wax was used to smooth any small steps between the windows and model skin. The model was supported with a rear-mounted, 0.75-m-long sting connected to a vertical post coming through the wind tunnel floor.

The location of transition on the prolate spheroid was found by Meier et al.[12] to be strongly dependent on freestream turbulence, and the stability of the separation on the prolate spheroid was found in the particle image velocimetry studies of Fu et al.[13] to be greatly enhanced by fixing the position of transition with a boundary layer-trip. Therefore, a circumferential trip, consisting of posts 1.2 mm in diameter and 0.7 mm high spaced 2.5 mm apart, was placed around the nose of the model at $x/L = 0.2$ to stabilize the location of transition and, consequently, the location of the separation. These posts were carefully sized to the boundary-layer thickness so that, using the analysis of Braslow and Knox,[14] little or no drag increase will result.

A unique, three-component, fiber-optic LDV probe was used for these measurements. It was designed specifically to measure the complete velocity vector and full Reynolds stress tensor from the viscous sublayer to the edge of the boundary layer on the 6:1 prolate spheroid. The design of the probe is discussed in detail in Ref. 10.

The probe is a two-color, three-component, fiber-optic design. Light for the probe comes from the blue and green lines of an argon-ion laser with scattered light collected in off-axis backscatter. The measured velocity components are mutually orthogonal, and the probe volume is roughly spherical with a diameter of approximately 55 μm. The probe was positioned inside the model with all beams passing through the window, as shown in Fig. 2. In this way the flow is undisturbed by the presence of the probe. The probe was mounted to the frame of the model on a two-component traverse, which could be remotely positioned $\pm$2.5 cm in both the axial and radial directions. Positioning in the circumferential, or ϕ, direction was accomplished by rotating the model about its primary axis. The Doppler frequency of the LDV signals was analyzed using three Macrodyne model FDP3100 frequency-domain signal processors operating in coincidence mode.

Polystyrene latex spheres 0.7 μm in diameter were used to seed the flow. The seed was suspended in ethanol and introduced into the flow using two air-atomizing paint spray nozzles placed just downstream of the turbulence-reducing screens. The arrangement of the two nozzles produced a localized region of seeded flow extending a minimum of 10 cm on all sides of the model. This arrangement causes some increase in the freestream turbulence; the increase, however, is below the measurement resolution of this instrument and has not been quantified.

In the window, approximately 1 mm to the windward (positive ϕ) circumferential side of the measurement volume, is a 0.5-mm pressure tap. An Endevco model 8507-C2 pressure transducer is placed just behind and to the side of this pressure tap. The transducer has a flat frequency response from 0 to 15 kHz. The short passage connecting the pressure tap to the transducer and the transducer dead

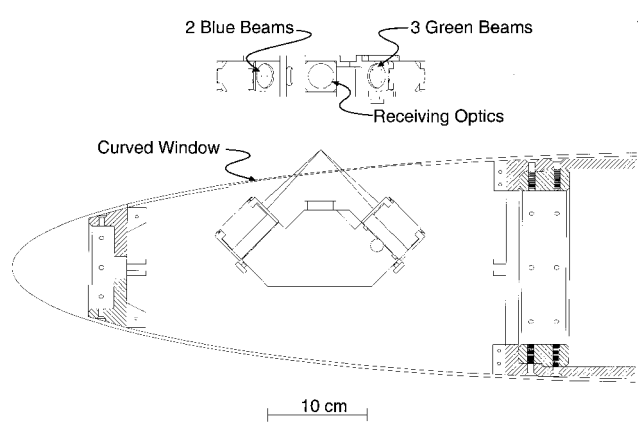

Fig. 2 Three-dimensional, fiber-optic, boundary-layer LDV probe placed inside the prolate spheroid.

volume result in a system resonant frequency at 11 kHz. With each particle velocity measurement, the pressure at the window pressure tap was sampled and stored with 16-bit precision.

All tests were performed at a Reynolds number based on the model length and freestream velocity of 4.20×10^6. Tests were performed at a 10-deg angle of attack at $x/L = 0.400$, 0.600, and 0.772. Surface oil-flow visualizations by Ahn[5] indicated that the primary separation is incipient at $x/L = 0.600$, $\alpha = 10$ deg and is well developed at $x/L = 0.772$. For $x/L = 0.772$, convergence of flow lines indicated the separation line to be at $\phi = 123$ deg. At 20-deg angle of attack, measurements were made at $x/L = 0.600$ and 0.772. The previous flow visualizations showed the separation to be much more pronounced at this angle of attack, with the primary separation well established at $x/L = 0.600$ and the secondary separation incipient. At $x/L = 0.772$, the secondary separation was well developed.

At each axial location, boundary-layer profiles were measured at from 10 to 14 circumferential locations from $\phi = 90$ to 180 deg. Each boundary-layer profile consisted of from 17 to 19 radial locations, from approximately 0.007 cm from the model surface out to 2.5–3.0 cm. At each of these locations, 16,384 coincident three-dimensional velocity/pressure realizations were acquired.

Uncertainty Estimates

Uncertainty estimates for the measurements presented are listed in Table 1. Errors due to velocity bias were corrected by using an inverse-velocity weighting scheme when calculating statistical averages, and uncertainties in the mean velocities due to finite sample size were small due to the large (16,384 points) sample size. The uncertainties in the mean velocities and the mean flow angles is then primarily due to calibration limitations and, therefore, should be considered bias uncertainties. Errors in the turbulence quantities due to gradient broadening were corrected using the scheme of Durst et al.[15] The primary source of uncertainty in these components arises from the uncertainty of calculating these higher-order statistical terms with a finite sample size. These uncertainties, therefore, should be considered random uncertainties. Uncertainty in the skin-friction coefficient arises primarily from uncertainties in the distance of the probe volume from the wall and uncertainties in the constants for a wall law fit of three-dimensional flows. Uncertainty in the skin friction, therefore, should be considered to be primarily a bias uncertainty. Turbulence quantities at the edge of the boundary layer are limited by a minimum measurable turbulence intensity of about 1.5%.

Table 1 Uncertainty estimates

Term	Uncertainty
U, V, W	$0.005\|U\|$
u_i^2	2%
β	0.7 deg
β_w	1.5 deg
γ_g	1.1 deg
γ_τ	4 deg
C_f	4%

Motion in the radial direction was powered by a rotary-encoded servomotor, and repeatability of the radial positioning was found to be better than ± 0.008 mm. Positioning of the measurement volume in the circumferential direction was measured with a sting-mounted index and was accurate to within 0.1 deg.

Results

Mean Velocity and Pressure Measurements

Figures 3–5 show the measured contours of total velocity overlaid with the secondary streamlines at $\alpha = 10$ deg, $x/L = 0.772$ and $\alpha = 20$ deg, $x/L = 0.600$ and 0.772 in planes perpendicular to the model axis. Also shown are plots of the wall-pressure coefficient measured at the same ϕ locations as the LDV profiles. The model surface is at the inner arc of the contoured region.

The secondary streamlines were calculated by interpolating the measured (V, W) vectors throughout the measured planes, and tracing the paths of imaginary particles in the interpolated field. These secondary streamlines clearly identify the separations, reattachments, and vortices that exist in the flowfield.

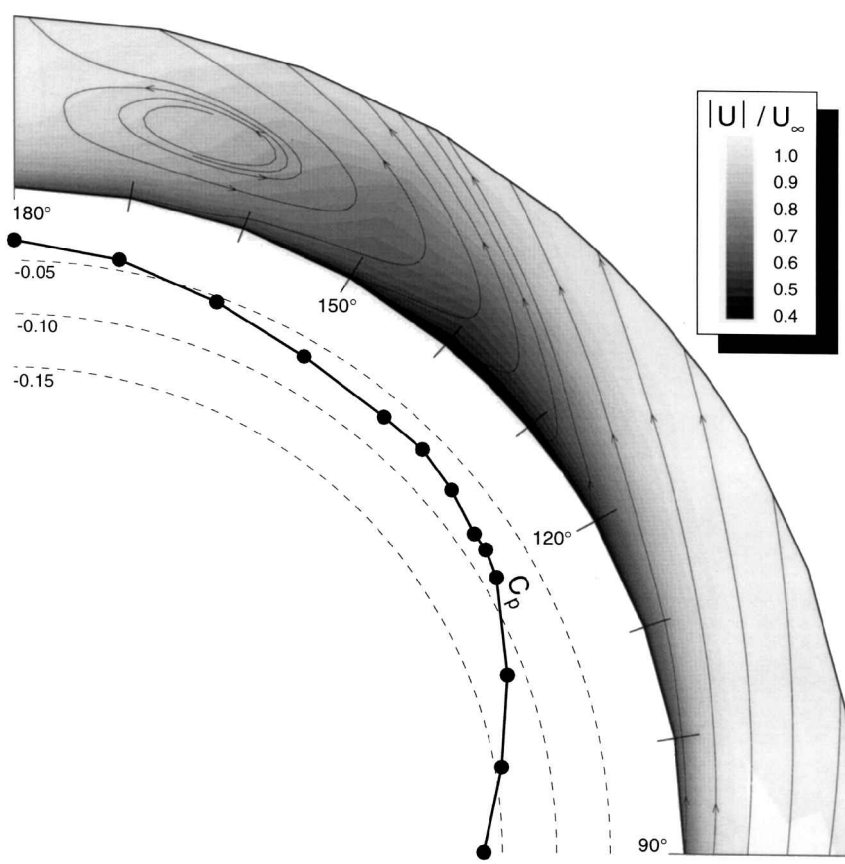

Fig. 3 Contours of total velocity with wall-pressure coefficient; $\alpha = 10$ deg, $x/L = 0.772$.

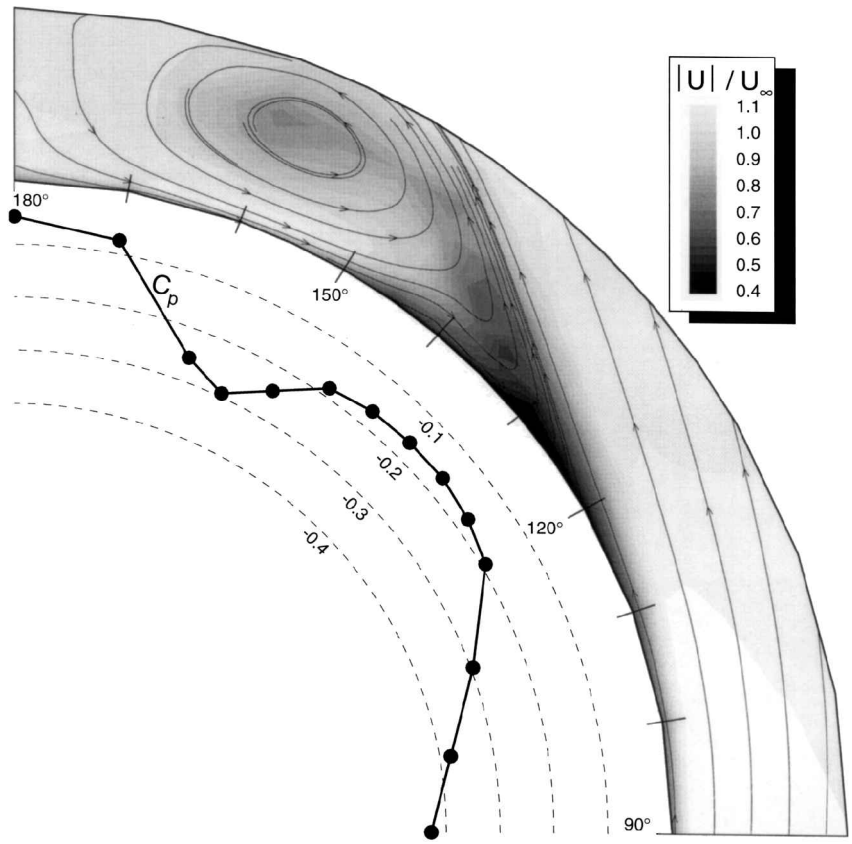

Fig. 4 Contours of total velocity with wall-pressure coefficient; α = 20 deg, *x*/*L* = 0.600.

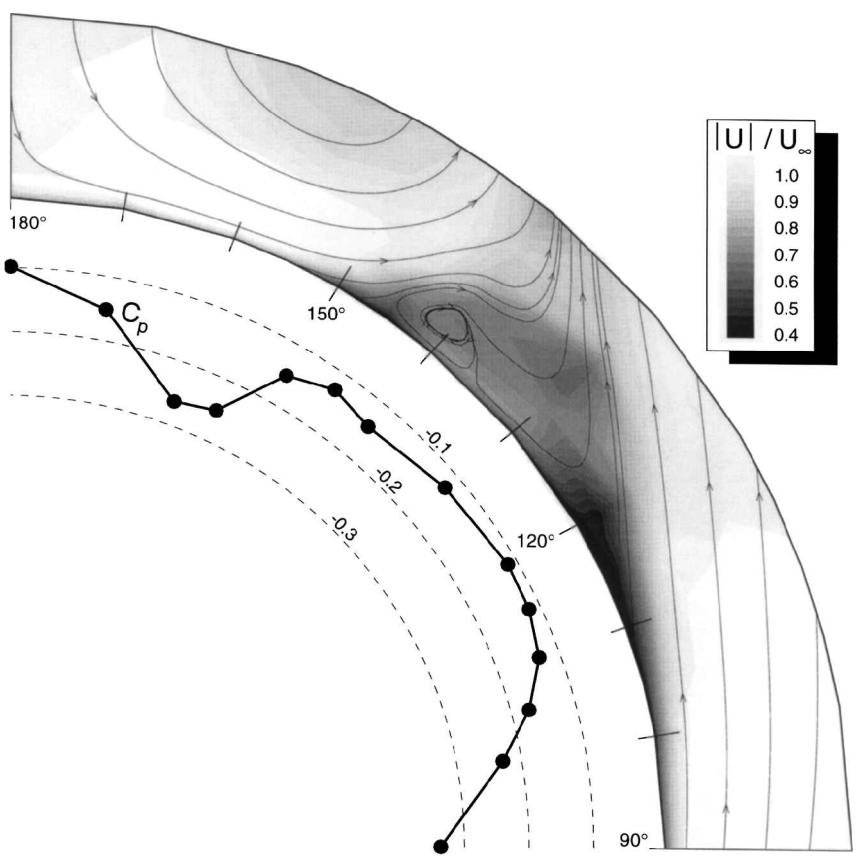

Fig. 5 Contours of total velocity with wall-pressure coefficient; α = 20 deg, *x*/*L* = 0.772.

In Fig. 3 ($\alpha = 10$ deg, $x/L = 0.772$), the streamlines reveal a single separation at $\phi = 123$ deg, accompanied by a vortex approximately 1.5 cm above the surface at $\phi = 165$ deg. Because this flow is symmetric about a vertical plane, there also exists another separation at $\phi = 237$ deg, another vortex is centered above $\phi = 195$ deg, and the point $\phi = 180$ deg is a reattachment.

In Fig. 4 ($\alpha = 20$ deg, $x/L = 0.600$), a single large vortex (the primary vortex) is centered about 1.8 cm above the model surface at $\phi = 158$ deg. This primary vortex is associated with the primary separation line, which is approximately at $\phi = 123$ deg. No secondary vortex or separation is clearly evident; however, the kink in the secondary streamlines just above the surface at $\phi = 140$ deg indicates that a secondary vortex may be starting to form at this location. Previous flow visualizations had, in fact, shown the secondary separation to be incipient at this axial location.

In Fig. 5 ($\alpha = 20$ deg, $x/L = 0.772$), the secondary vortex is clearly evident at $\phi = 140$ deg, and the associated secondary separation and reattachment are seen at $\phi = 147$ and 135 deg, respectively. The primary vortex has moved away from the surface of the model, and the primary separation has moved down to $\phi = 112$ deg.

Plots of the secondary streamlines for $\alpha = 10$ deg, $x/L = 0.600$, which are not shown here but are plotted later, reveal separation just beginning with a very small primary vortex just above the surface at $\phi = 162$ deg. Plots of the secondary streamlines for $\alpha = 10$ deg, $x/L = 0.400$ are not shown here at all because they reveal no separations or vortices.

The plots of C_p in Figs. 3–5 show the pressure to be lowest at $\phi = 90$ deg, where the flow has been accelerated around the model. The pressure then rises past $\phi = 90$ deg until separation is reached; the pressure becomes almost flat past the separation. For the two $\alpha = 20$-deg cases, the influence of the primary vortex on the wall pressure is quite strong. In both cases the wall pressure is at a local minimum directly below the primary vortex. After the flow passes under the primary vortex (moving in the $-\phi$ direction), the pressure rises. The rise in pressure past the primary vortex then leads to the secondary separation.

The contours of total velocity in Figs. 3–5 show the highest velocity fluid to be on the side of the prolate spheroid ($\phi = 90$ deg), where the flow has accelerated around the model, and underneath the primary vortex, particularly at $\alpha = 20$ deg, $x/L = 0.772$. The lowest velocities exist just downstream of the separation lines. For the two $\alpha = 20$-deg cases it is clear that a trough of low-velocity fluid has formed between the two separation lines, corresponding to the regions where C_p is approximately constant. The fluid in this region is convecting out to the sides. Because this fluid is not being replaced from the fluid above (V is not negative), continuity demands that the streamwise component of velocity must decrease. The same creation of a low-velocity zone appears in a less dramatic fashion at $\alpha = 10$ deg, $x/L = 0.772$, where there is only one separation line.

An alternate, but not conflicting, explanation for the accumulation of low-velocity fluid downstream of the separations is that the vortices, which form past the separations, sweep up the low-momentum fluid near the wall and that this fluid then accumulates between the vortex and the separation line. When the vortex is strong, some of the low-velocity fluid gets pulled out of the region near the wall and into the vortex itself. This can be seen clearly in Fig. 4, where a finger of low-velocity fluid stretches from the wall out to the center of the vortex, and also in Fig. 5, where the same phenomenon appears to be present, but is somewhat obscured by the vortex moving out of the measured region.

Skin Friction and Wall-Flow Angle

To calculate the skin friction, the velocity profiles were fitted to a Spalding type wall law

$$y^+ = u^+ + \frac{1}{E}\left[e^{\kappa u^+} - 1 - \kappa u^+ - \frac{(\kappa u^+)^2}{2} - \frac{(\kappa u^+)^3}{6}\right] \qquad (1)$$

with the constants $E = 8.323$ and $\kappa = 0.41$ and with the substitutions

$$u^+ = \frac{U_{wc}/U_\infty}{\sqrt{C_f/2}} \qquad y^+ = \frac{y + \Delta y}{L} Re_L \sqrt{\frac{C_f}{2}} \qquad (2)$$

This equation satisfies the continuity equation requirements of Rotta[16] that $u^+ - y^+$ vary as y^{+4} nearest the wall while u^+ approaches a semilogarithmic form for large y^+. In this way, the skin-friction coefficient, and the term Δy, can be calculated from a least squares fit of this equation to the measured U_{wc}/U_e vs y/L pairs. (Δy is a term correcting for any small error in the traverse zero point and was typically less than 30 μm.) This equation is, strictly, only applicable to two-dimensional flows. However, in a study of three-dimensional boundary layers, Ölçmen and Simpson[17] found that the region of flow below $y^+ = 100$ is dominated by laminar wall flow and follows a two-dimensional wall law reasonably well. For these three-dimensional profiles then, only the points measured within the region below $y^+ = 100$ are used for the least squares fit.

The magnitude of the measured skin-friction coefficient C_f is plotted in Fig. 6, and the direction of the flow at the wall relative to the axial direction, β_w, is plotted in Fig. 7. C_f has been normalized by the wind tunnel velocity U_∞ to make comparisons between different measurement locations more convenient.

The minima in skin friction in Fig. 6 do not occur exactly at the separation locations, but rather occur some distance downstream of the separation lines, in agreement with the hot-film prolate spheroid measurements of Meier and Kreplin.[18] The minima do correspond very well, however, to the regions of low-velocity fluid near the wall seen in Figs. 3–5. Although the minima in skin friction roughly correspond to the separation lines, the flow at $\alpha = 20$ deg, $x/L = 0.772$ has two minima and two separation lines, the flow at $\alpha = 20$ deg, $x/L = 0.600$ has one pronounced minimum and one weak minimum corresponding to a well-developed separation and an incipient separation, and the flows at $\alpha = 10$ deg, $x/L = 0.600$ and 0.772 both have a single minimum and a single separation; the skin friction minima are not precise indicators of separation location. The flow at $\alpha = 10$ deg, $x/L = 0.400$, for example, has a weak local minimum in skin friction at $\phi = 150$ deg but has no separation. Similarly, the local maxima cannot be relied on to indicate reattachment. Although there exists a local maxima in the skin friction at $\alpha = 20$ deg,

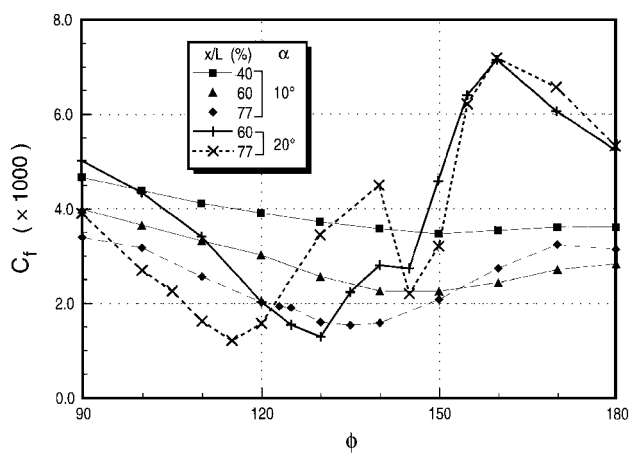

Fig. 6 Skin friction on the prolate spheroid.

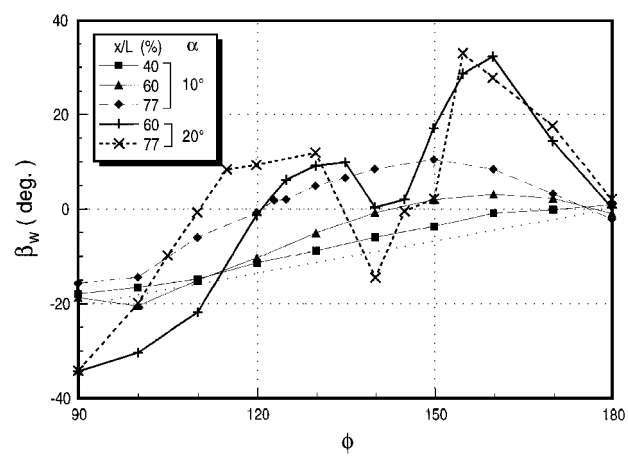

Fig. 7 Wall-flow angle on the prolate spheroid.

$x/L = 0.772$ near the secondary reattachment point, for example, there also exists a larger maxima at $\phi = 160$ deg corresponding not to a reattachment but rather to the primary vortex. The reattachment at $\phi = 180$ deg actually occurs at a minimum in skin friction. The skin friction is then useful in determining the structure of the flow only when combined with other information, such as the velocity field.

In Fig. 7, the wall-flow angle at $\phi = 90$ deg is approximately from −16 to −19 deg for all cases at $\alpha = 10$ deg and is about −35 deg for the $\alpha = 20$-deg cases. For all cases, the flow angle is approximately 0 deg at $\phi = 180$ deg, as symmetry demands. On a plot of wall-flow angle, the feature that would distinguish a separation or reattachment would be a discontinuity in the plot. In Fig. 7 there do appear to be discontinuities in the plot near some of the separation and reattachment points, particularly for $\alpha = 20$ deg, $x/L = 0.772$. However, detection of separation and reattachment lines by this method requires very close spacing of the measurement locations in the cross-stream direction. The spacing of the measurements in the ϕ direction in these plots is not sufficient to identify the lines from β_w alone.

Turbulent Kinetic Energy and Wall-Pressure Fluctuations

Figures 8 and 9 show the measured contours of twice the TKE q^2 overlaid with the secondary streamlines at $\alpha = 20$ deg, $x/L = 0.600$ and 0.772 along with plots of the measured wall-pressure fluctuations, p. The plots of p/Q include both acoustic and turbulent pressure fluctuations because with these data no spectral information was available. The subtraction of acoustic pressure fluctuations from this data should only reduce the magnitude of p/Q slightly and should do so approximately evenly for all locations. Therefore, the shape of the p/Q plots should not be influenced by the acoustic pressure fluctuations.

The contours of TKE show that the lifting of the secondary streamlines at separation is accompanied by the lifting of a sheet of very turbulent fluid. This sheet appears to be drawn by the primary vortex from the boundary layer into the vortex core.

Downstream of the separation lines, the fluid near the wall exhibits extremely low-turbulence levels. For the case of $\alpha = 20$ deg, $x/L = 0.772$, the primary separation line is approximately at $\phi = 112$ deg. The TKE just downstream of the separation at $\phi = 115$ deg is lower at $y^+ = 10$ (normally the location of the peak turbulence) than the TKE just upstream of the separation at $\phi = 110$ deg is at $y^+ = 500$. The turbulence near the wall increases again at the reattachment ($\phi = 135$ deg), but is nearly as low at $\phi = 145$ deg, just downstream of the secondary separation.

This low TKE just downstream of the separation lines is echoed in the measurements of the fluctuating component of the wall pressure p. For $\alpha = 20$ deg, $x/L = 0.772$, p reaches a minimum at $\phi = 120$ deg, very near the location of the minimum in TKE. The fluctuating pressure level rises at the secondary reattachment point, but then reaches another minimum at $\phi = 145$ deg, just downstream of the secondary separation.

A similar phenomenon is exhibited in Fig. 8, which shows at $\alpha = 20$ deg, $x/L = 0.600$ that the TKE behind the separation line reaches a minimum at $\phi = 130$ deg, as does the fluctuating pressure level. At $\alpha = 10$ deg, $x/L = 0.772$, a location with only a single separation, the velocity and pressure fluctuations reach a minimum downstream of the separation line as well. There, the TKE reaches a local minimum at $\phi = 135$ deg, and p reaches a minimum at 140 deg.

The separations then generate regions just downstream that are quite distinct from the rest of the flow. They have both low mean kinetic energy (low $|U|$) and low fluctuating kinetic energy (low q^2). This trough of relatively quiescent fluid is, in the case of a single separation, wedged between the separation line and the primary vortex or, in the case of two separation lines, contained between the two separation sheets.

Helicity Density

The vorticity in a flow can be divided into two components: the streamwise vorticity characteristic of three-dimensional flow structures and the cross-stream vorticity characteristic of two-dimensional shear layers. The helicity h, which is the dot product of the vorticity and the velocity, can be used as a means of identifying streamwise vorticity and, thus, can be used to locate vortices. As will presently be shown, it can also be used to identify a three-dimensional separation.

The contours of h are shown for $\alpha = 20$ deg, $x/L = 0.772$ in Fig. 10. The white line marks the contour of zero helicity. The

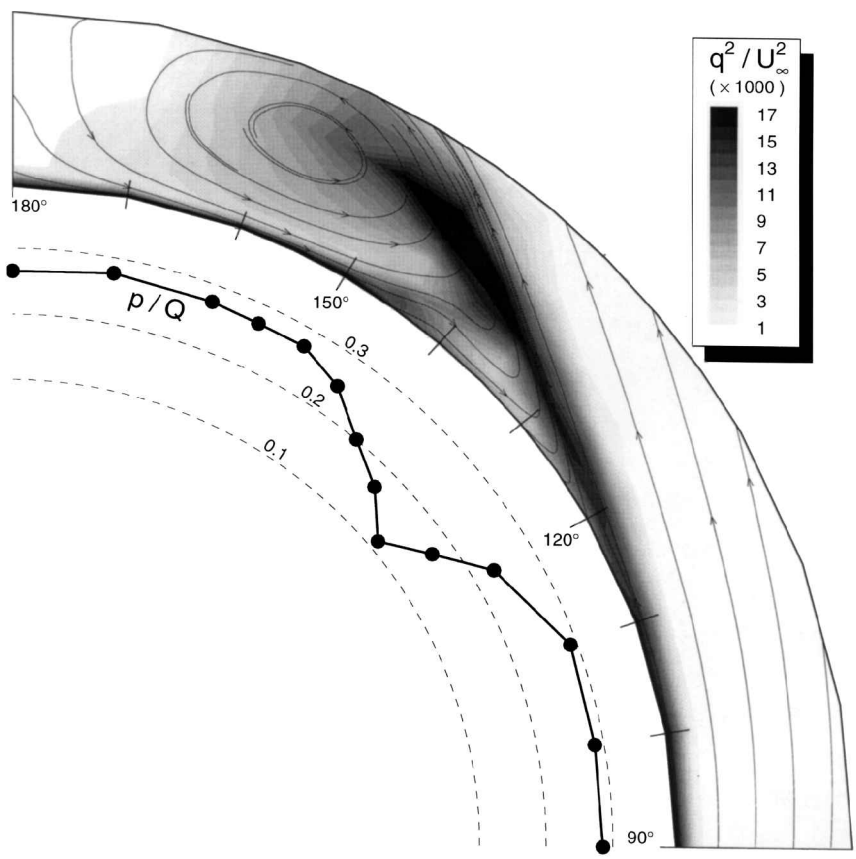

Fig. 8 Contours of TKE with wall-pressure fluctuations; $\alpha = 20$ deg, $x/L = 0.600$.

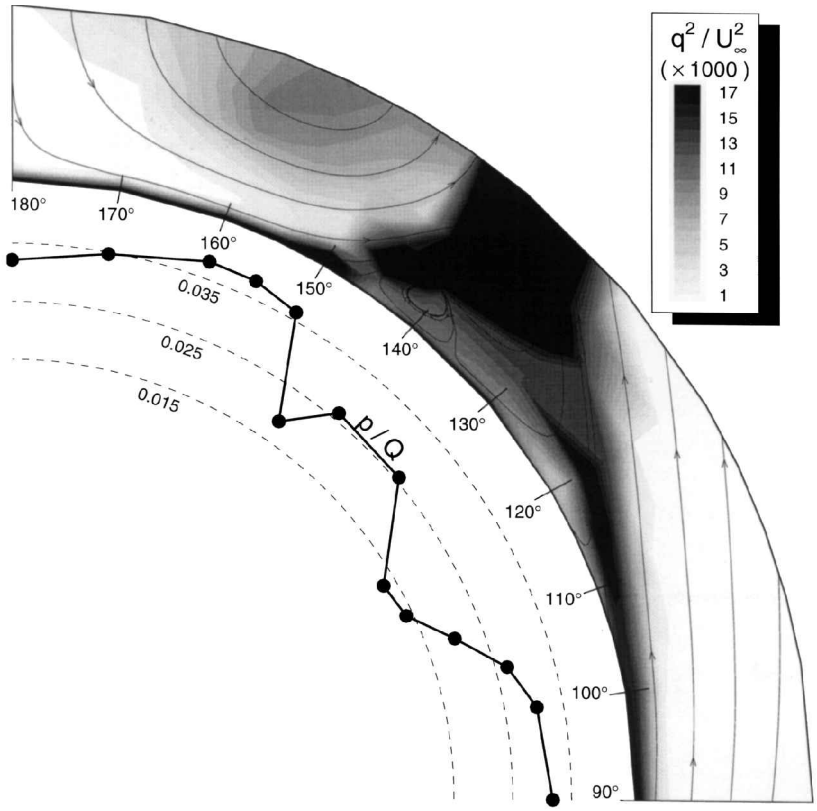

Fig. 9 Contours of TKE with wall-pressure fluctuations; α = 20 deg, x/L = 0.772.

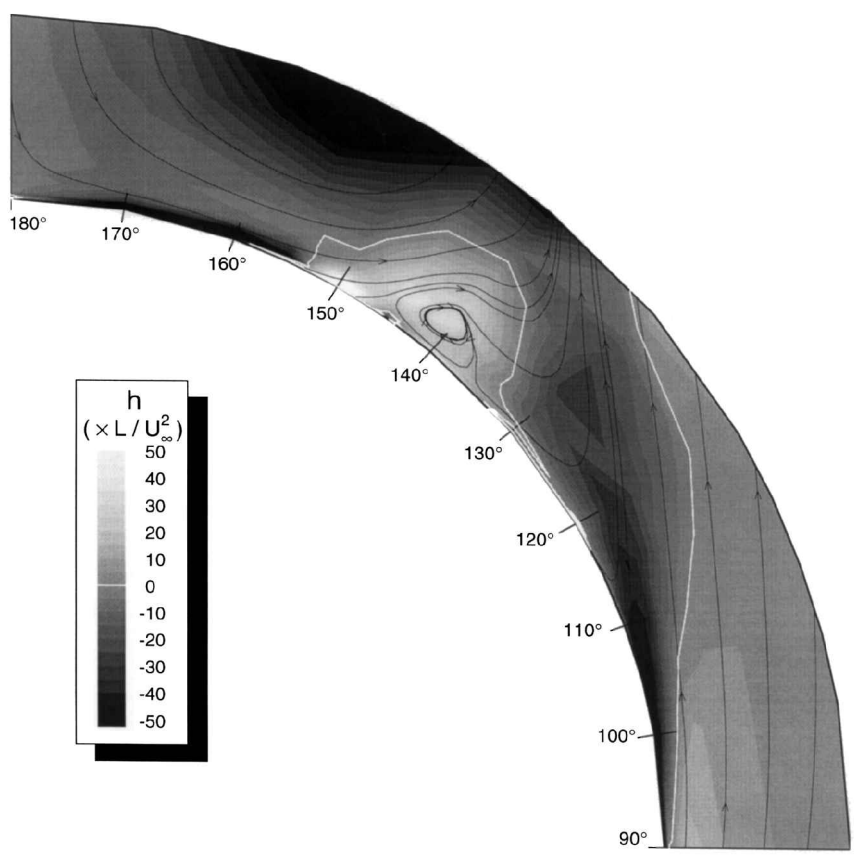

Fig. 10 Contours of helicity density; α = 20 deg, x/L = 0.772.

contours show a region of large positive helicity, where the secondary streamlines show the secondary vortex to be, and a large negative helicity near the center of the primary vortex. There is a sheet of high-helicity fluid emanating from the surface at $\phi = 110$ deg, just upstream of the primary separation, which extends toward the primary vortex, and a sheet of high negative helicity fluid emanating from the surface at $\phi = 150$ deg, just upstream of the secondary separation, which extends toward the secondary vortex. Near the surface of the model, the helicity changes sign very close to the separation lines.

Turbulence Anisotropy

Currently, the great majority of turbulent flow codes in use employ turbulence models that assume an isotropic eddy viscosity; that is, they assume that the turbulent-shear-stress vector is some scalar multiple of the flow-gradient vector. In mathematical notation this is expressed as

$$N = \left(\frac{\overline{vw}}{\overline{uv}}\right) \Big/ \left(\frac{\partial U/\partial y}{\partial W/\partial y}\right) \equiv 1 \tag{3}$$

or, identically, that the turbulent-shear-stress angle γ_τ is equal to the flow-gradient angle γ_g, where

$$\gamma_g = a\tan\left(\frac{\partial W/\partial y}{\partial U/\partial y}\right) \qquad \gamma_\tau = a\tan\left(\frac{\overline{vw}}{\overline{uv}}\right) \tag{4}$$

Two general types of turbulence models exist that do not assume that the eddy viscosity is isotropic. The first of these are the models that solve a separate partial differential equation for each of the Reynolds stresses. The most notable of these Reynolds stress, or second-moment closure, models is that of Gibson and Launder,[19] but several other variations of the scheme exist. These models make no assumption about the value of N, because they make no use of an eddy viscosity concept. They are very little in use, however, due to their computational complexity and cost. The second type of models that do not use an isotropic eddy viscosity are models that utilize an eddy viscosity, but allow N to vary from the isotropic value of 1. The most notable of these is the Rotta-T model.[20] In the Rotta-T model, T, which is identical to N when defined relative to the streamwise direction, is assumed to be a constant not equal to 1.

To judge the applicability of these models to three-dimensional, separating flows, the quantity $|\gamma_g - \gamma_\tau|$ is plotted for $\alpha = 10$ deg, $x/L = 0.600$ and $\alpha = 20$ deg, $x/L = 0.600$ and 0.772 in Figs. 11–13. This quantity can be related to N (or T) by

$$N = 1 - \tan(\gamma_g - \gamma_\tau)\left[\frac{1}{\tan\gamma_g} + \tan\gamma_\tau\right] \tag{5}$$

and has the benefits that 1) unlike N it is coordinate system invariant and 2) unlike both T and N it does not blow up when the flow-gradient angle is zero. As $|\gamma_g - \gamma_\tau|$ moves away from zero, the eddy viscosity becomes less isotropic.

In Fig. 11, it can be seen that for $\alpha = 10$ deg, $x/L = 0.600$, the shear-stress angle and the flow-gradient angle are closely aligned throughout the boundary layer. (Outside of the boundary layer, where the turbulence is very low, the uncertainty on γ_τ is very high, and the fluctuations in the contours should be ignored.) At this station, the three dimensionality of the flow is very mild and has not much affected the turbulence structure. In Fig. 12, $\alpha = 20$ deg, $x/L = 0.600$, the shear-stress angle and the flow-gradient angle are aligned over most of the boundary layer, but it is clear that in some regions, most notably underneath the primary vortex, near where the secondary vortex is forming, and along the primary separation sheet, γ_g and γ_τ are becoming significantly misaligned. In Fig. 13, $\alpha = 20$ deg, $x/L = 0.772$, the shear-stress angle and the flow-gradient angle have become severely misaligned over much of the flow. Over large regions, γ_g and γ_τ differ by more than 90 deg indicating that there is no relation between the streamwise and cross-stream eddy viscosities.

It is clear then that for mildly three-dimensional flows, such as the flow at $\alpha = 10$ deg, $x/L = 0.600$, isotropic eddy viscosity models will describe the flow adequately. As the flow becomes increasingly dominated by three-dimensional structures, the isotropic eddy viscosity models will perform increasingly poorly. The results here for

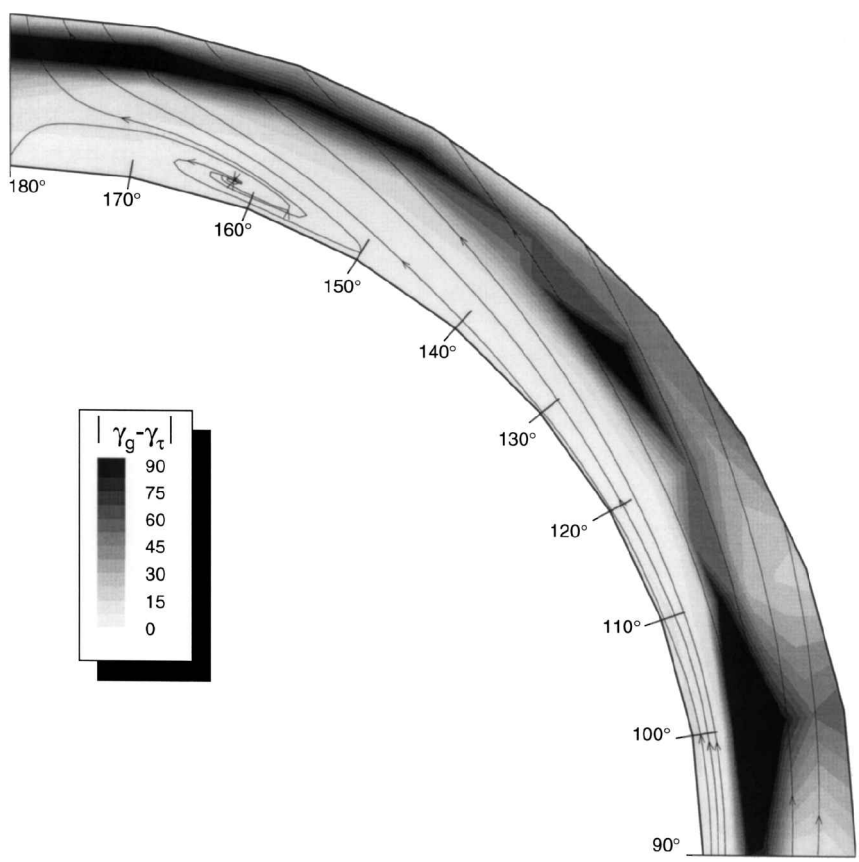

Fig. 11 Contours of turbulence anisotropy; $\alpha = 10$ deg, $x/L = 0.600$.

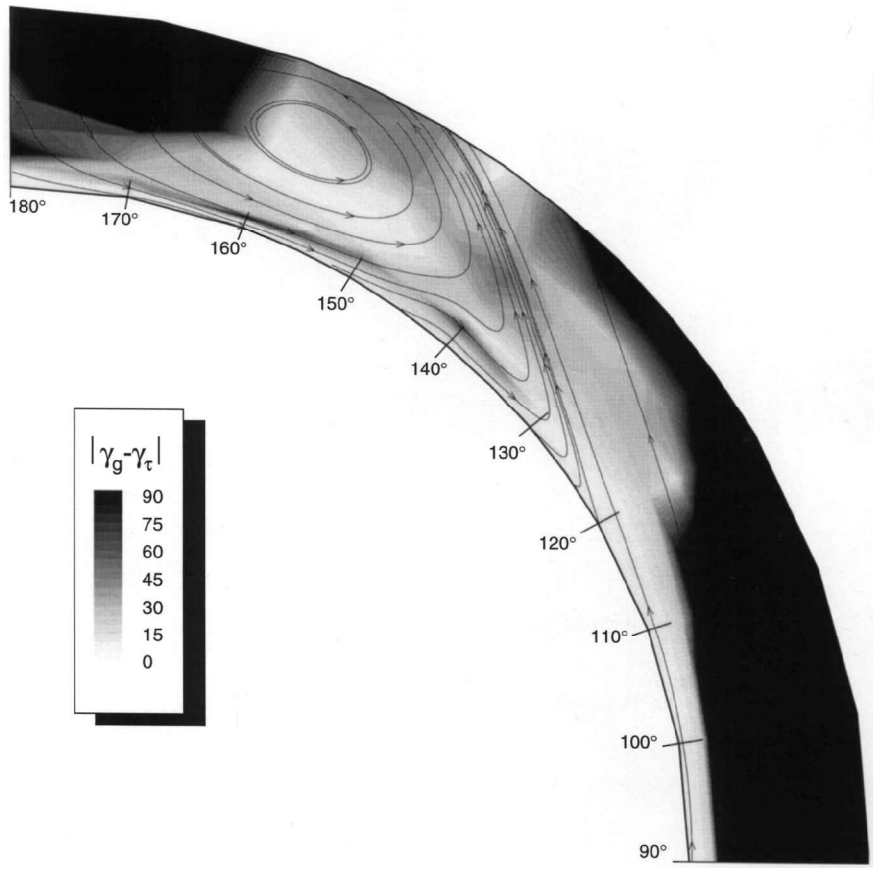

Fig. 12 Contours of turbulence anisotropy; α = 20 deg, x/L = 0.600.

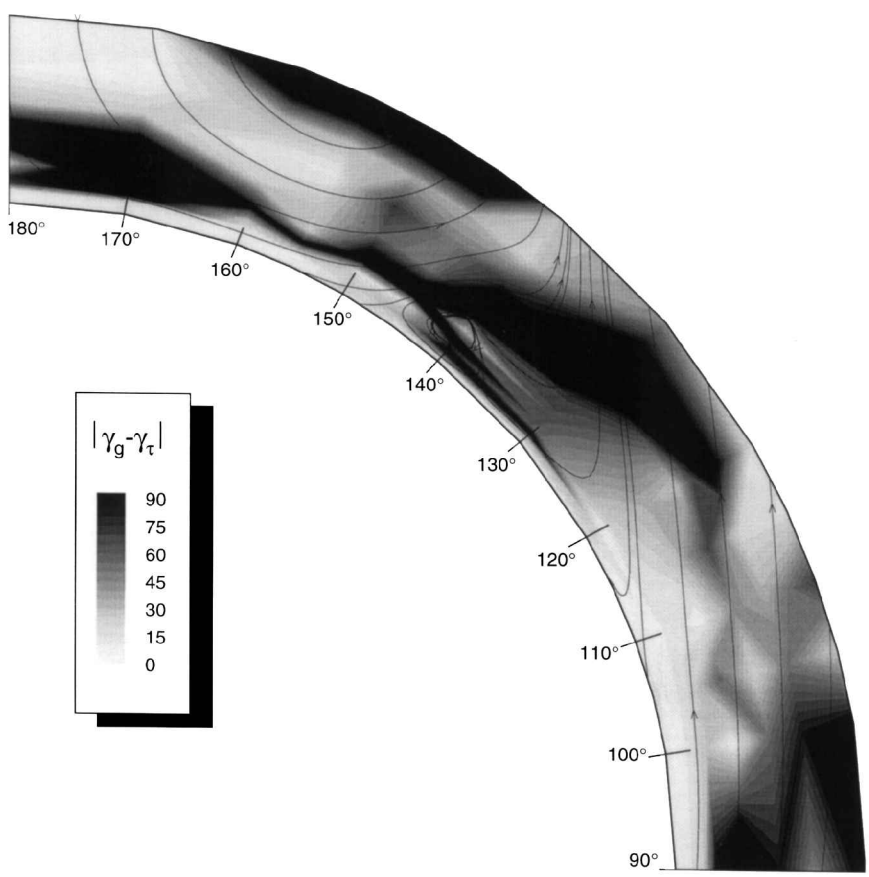

Fig. 13 Contours of turbulence anisotropy; α = 20 deg, x/L = 0.772.

$\alpha = 20$ deg, $x/L = 0.772$ show that for highly three-dimensional flows, isotropic eddy viscosity models are inappropriate. The Rotta-T model is inappropriate as well because for large regions of the flow there is no relation between the streamwise and cross-stream eddy viscosity. The only models that are appropriate for strongly three-dimensional flows are those that solve for the Reynolds stresses.

Summary and Conclusions

A miniature, three-dimensional, fiber-optic LDV was used to survey the separating flowfield about an inclined 6:1 prolate spheroid at a Reynolds number based on model length of 4.2×10^6. Measurements were made on the leeward side of the model at $\alpha = 10$ deg, $x/L = 0.400$, 0.600, and 0.772, and at $\alpha = 20$ deg, $x/L = 0.600$ and 0.772. These measurements extended from less than 0.007 cm from the model surface out to beyond the boundary-layer edge. Simultaneous with the three-dimensional LDV measurements were measurements of the surface pressure just below the measurement volume.

The measurements revealed several techniques for finding the separation and reattachment points on the model. The clearest of these was the generation of secondary streamlines from the measured velocity field. The secondary streamlines reveal not only the separations and reattachments, but also reveal the vortical structures in the flow. Unfortunately, to generate the secondary streamlines requires a great number of accurate velocity measurements.

Measurements of the skin friction were shown to be somewhat imprecise indicators of the separation. Minima in skin friction generally occur some distance downstream of the separation line, but may sometimes occur even when no separation is present. Skin-friction maxima are a poor indicators of reattachment. Maxima can occur for other reasons, such as underneath a vortical structure, and reattachment often occurs without the presence of a local skin-friction maximum.

Measurements of the wall-flow angle can be used to find the separation and reattachment points in flows such as this, but, in practice, it is time-consuming and tedious. At the three-dimensional separation and reattachment lines, there should be a discontinuity in the flow angle. Because these discontinuities can be small, to find them requires very closely spaced, accurate measurements of the wall flow angle. This can be achieved much more simply by use of an oil-flow technique.

Other measurements that can reveal the location of separation are turbulent kinetic energy, which drops significantly across the separation but may take some distance to do so if the separation is not strong; helicity; density, which changes sign very near the separation point but may be difficult to measure; and wall-pressure coefficient, plots of which will become almost flat past the separation line. It is clear that none of these techniques is completely reliable in revealing the separation topology and that multiple techniques may need to be employed.

Investigation of the flow structure in the vicinity of the three-dimensional separations revealed a region just behind the separation lines that is quite distinct from the rest of the flow. A trough of fluid exists, which is located between the primary vortex and the separation sheet in the case of a single separation, and between the two separation sheets in the case of two separations, that is relatively quiescent. The fluid has relatively low velocity and low turbulence. The flow near the wall at $\alpha = 20$ deg, $x/L = 0.772$ was found to have turbulence levels just behind the primary separation one-third of those just ahead of separation. The vortex formed by the separation, if strong, may pull some of the fluid away from the surface and in toward its core.

Measurements of the flow-gradient angle γ_g and the turbulent-shear-stress angle γ_τ reveal that, for mildly three-dimensional flows, the two angles are nearly equal, and models that assume an isotropic eddy viscosity should be sufficient. In highly three-dimensional flows with multiple three-dimensional separations, large regions of the flow have γ_g and γ_τ strongly misaligned. This implies that models that use an isotropic eddy viscosity are incapable of adequately describing these flows. Models that use an anisotropic eddy viscosity model, such as the Rotta-T model, are insufficient as well, because large regions of the flow have no correlation between the flow-gradient and the turbulent-shear-stress angles. For highly three-dimensional flows, the eddy viscosity concept is simply inappropriate. The best hopes for modeling these flows are models that solve a partial differential equation for each of the turbulent shear stresses.

Acknowledgment

The authors appreciate the support of this work by the Office of Naval Research, Grant N00014-94-1-0092, L. P. Purtell, Program Manager.

References

[1] Meier, H. U., Kreplin, H. P., Landhaußer, A., and Baumgarten, D., "Mean Velocity Distributions in Three-Dimensional Boundary Layers Developing on a 1:6 Prolate Spheroid with Natural Transition," DFVLR, Data Rept. DFVLR IB 222-4/A 10, Göttingen, Germany, 1984.

[2] Meier, H. U., Kreplin, H. P., and Landhaußer, A., "Wall Pressure Measurements on a 1:6 Prolate Spheroid in the DFVLR 3 m × 3 m Low Speed Wind Tunnel ($\alpha = 10°$, $U_\infty = 55$ m/s, Artificial Transition)," DFVLR, Data Rept. DFVLR IB 222-86 A 04, Göttingen, Germany, 1986.

[3] Kreplin, H. P., Vollmers, H., and Meier, H. U., "Wall Shear Stress Measurements on an Inclined Prolate Spheroid in the DFVLR 3 m × 3 m Low Speed Wind Tunnel," DFVLR, Data Rept. DFVLR IB 222-84/A 33, Göttingen, Germany, 1985.

[4] Vollmers, H., Kreplin, H. P., Meier, H. U., and Kühn, A., "Measured Mean Velocity Field Around a 1:6 Prolate Spheroid at Various Cross Sections," DFVLR, Data Rept. DFVLR IB 221-85 A 08, Göttingen, Germany, 1985.

[5] Ahn, S., "An Experimental Study of Flow over a 6 to 1 Prolate Spheroid at Incidence," Ph.D. Dissertation, Dept. of Aerospace and Ocean Engineering, Virginia Polytechnic Inst. and State Univ., Blacksburg, VA, Oct. 1992.

[6] Barber, K. M., and Simpson, R. L., "Mean Velocity and Turbulence Measurements of Flow Around a 6:1 Prolate Spheroid," AIAA Paper 91-0255, Jan. 1991.

[7] Anon., "Calculation of 3D Separated Turbulent Flows in Boundary Layer Limit," AGARD-AR-255, Neuilly sur Seine, France, May 1990.

[8] Gee, K., Cummings, R. M., and Schiff, L. B., "Turbulence Model Effects on Separated Flow About a Prolate Spheroid," *AIAA Journal*, Vol. 30, No. 3, 1992, pp. 655–664.

[9] Chesnakas, C. J., and Simpson, R. L., "Measurements of the Turbulence Structure in the Vicinity of a 3-D Separation," *Journal of Fluids Engineering*, Vol. 118, No. 2, 1996, pp. 268–275.

[10] Chesnakas, C. J., and Simpson, R. L., "Full Three-Dimensional Measurements of the Cross-Flow Separation Region of a 6:1 Prolate Spheroid," *Experiments in Fluids*, Vol. 17, No. 1/2, 1994, pp. 68–74.

[11] Chesnakas, C. J., Simpson, R. L., and Madden, M. M., "Three-Dimensional Velocity Measurements on a 6:1 Prolate Spheroid at 10° Angle of Attack," Dept. of Aerospace and Ocean Engineering, Data Rept. VPI-AOE-202, Virginia Polytechnic Inst. and State Univ., Blacksburg, VA, Jan. 1994.

[12] Meier, H. U., Michel, U., and Kreplin, H. P., "The Influence of Wind Tunnel Turbulence on the Boundary Layer Transition," *Perspectives in Turbulence Studies*, DFVLR, Göttingen, Germany, 1987, pp. 26–46.

[13] Fu, T. C., Shekarriz, A., Katz, J., and Huang, T. T., "The Flow Structure in the Lee of an Inclined 6:1 Prolate Spheroid," *Journal of Fluid Mechanics*, Vol. 269, June 1994, pp. 79–106.

[14] Braslow, A. L., and Knox, E. C., "Simplified Method for Determination of Critical Height of Distributed Roughness Particles for Boundary-Layer Transition at Mach Numbers from 0 to 5," NACA TN 4363, Sept. 1958.

[15] Durst, F., Martinuzzi, R., Sender, J., and Thevenin, D., "LDA Measurements of Mean Velocity RMS-Values and Higher Order Moments of Turbulence Intensity Fluctuations in Flow Fields with Strong Velocity Gradients," *Proceedings of the Sixth International Symposium on Applications of Laser Techniques to Fluid Mechanics* (Lisbon Portugal), Instituto Superior Tecnico, Lisbon, Portugal, 1992, pp. 5.1.1–5.1.6.

[16] Rotta, J. C., "Turbulent Boundary Layers in Incompressible Flow," *Progress in Aeronautical Sciences*, edited by A. Ferri, D. Küchemann, and L. H. G. Sterne, Vol. 2, Macmillan, New York, 1962, pp. 1–220.

[17] Ölçmen, M. S., and Simpson, R. L., "Perspective: On the Near Wall Similarity of Three-Dimensional Turbulent Boundary Layers," *Journal of Fluids Engineering*, Vol. 114, Dec. 1992, pp. 487–495.

[18] Meier, H. U., and Kreplin, H. P., "Experimental Investigation of the Boundary Layer Transition and Separation on a Body of Revolution," *Zeitschrift fuer Flugwissenschaften und Weltraumforschung*, Vol. 4, No. 2, 1980, pp. 65–71.

[19] Gibson, M. M., and Launder, B. E., "Ground Effects on Pressure Fluctuations in the Atmospheric Boundary Layer," *Journal of Fluid Mechanics*, Vol. 86, June 1978, pp. 491–511.

[20] Rotta, J. C., "A Family of Turbulence Models for Three-Dimensional Boundary Layers," *Turbulent Shear Flows 1*, edited by F. Durst, B. E. Launder, F. W. Schmidt, and J. H. Whitelaw, Springer–Verlag, Berlin, 1979, pp. 267–278.

F. W. Chambers
Associate Editor